Komander D, Lord CJ, Scheel H, Swift S, Hofmann K, Ashworth A et al.. The structure of the CYLD USP domain explains its specificity for Lys63-linked polyubiquitin and reveals a B b...

ARTICLE *in* MOLECULAR CELL · MARCH 2008

Impact Factor: 14.02 · DOI: 10.1016/j.molcel.2007.12.018 · Source: PubMed

Molecular Cell
Article

The Structure of the CYLD USP Domain Explains Its Specificity for Lys63-Linked Polyubiquitin and Reveals a B Box Module

David Komander,[1] Christopher J. Lord,[2] Hartmut Scheel,[3] Sally Swift,[2] Kay Hofmann,[3] Alan Ashworth,[2] and David Barford[1,*]
[1]Section of Structural Biology
[2]The Breakthrough Breast Cancer Research Centre
Institute of Cancer Research, Chester Beatty Laboratories, 237 Fulham Road, London SW3 6JB, UK
[3]Miltenyi Biotec GmbH, MACSmolecular Business Unit, Stöckheimer Weg 1, 50829 Cologne, Germany
*Correspondence: david.barford@icr.ac.uk
DOI 10.1016/j.molcel.2007.12.018

SUMMARY

The tumor suppressor CYLD antagonizes NF-κB and JNK signaling by disassembly of Lys63-linked ubiquitin chains synthesized in response to cytokine stimulation. Here we describe the crystal structure of the CYLD USP domain, revealing a distinctive architecture that provides molecular insights into its specificity toward Lys63-linked polyubiquitin. We identify regions of the USP domain responsible for this specificity and demonstrate endodeubiquitinase activity toward such chains. Pathogenic truncations of the CYLD C terminus, associated with the hypertrophic skin tumor cylindromatosis, disrupt the USP domain, accounting for loss of CYLD catalytic activity. A small zinc-binding B box domain, similar in structure to other crossbrace Zn-binding folds—including the RING domain found in E3 ubiquitin ligases—is inserted within the globular core of the USP domain. Biochemical and functional characterization of the B box suggests a role as a protein-interaction module that contributes to determining the subcellular localization of CYLD.

INTRODUCTION

Mutations of the tumor suppressor gene *CYLD* are the cause of a genetic predisposition to familial cylindromatosis, a hypertrophic skin cancer affecting predominantly hair follicles and sweat glands of the head and neck (Biggs et al., 1995; Bignell et al., 2000; Ikeda and Dikic, 2006; van Balkom and Hennekam, 1994). The protein product of *CYLD* is a deubiquitinase (DUB) specific for the disassembly of Lys63-linked ubiquitin polymers, a function mediated by its C-terminal USP domain (Brummelkamp et al., 2003; Kovalenko et al., 2003; Trompouki et al., 2003). Premature protein truncations that disrupt the USP domain, and therefore inactivate the capacity of CYLD to cleave Lys63-linked polyubiquitin, constitute the vast majority of cylindromatosis-associated mutations (Bignell et al., 2000).

CYLD negatively regulates activation of the cell-survival effector NF-κB, a finding that links its genetic characterization as a tumor suppressor to a cellular phenotype (Ikeda and Dikic, 2006). This function of CYLD combines its DUB activity with the emerging nonproteolytic role of Lys63-linked polyubiquitination as an effector of ligand-stimulated intracellular signaling and protein kinase activation (Chen, 2005; Deng et al., 2000; Sun and Chen, 2004). Studies of Cyld-deficient mice have implicated the protein as a suppressor of the Lys63-linked polyubiquitin-mediated processes responsible for stimulation of NF-κB and JNK in the innate and adaptive immune response (Jin et al., 2007; Zhang et al., 2006). Cyld-deficient mice developed severe colonic inflammation and exhibited enhanced induction of tumors of the colon (Zhang et al., 2006), findings that appear to correlate with reduced expression of CYLD in human colorectal cancers (Hellerbrand et al., 2007). In keratinocytes, the Lys63 deubiquitinating activity of CYLD is thought to be responsible for inhibiting tumorigenesis by suppressing Bcl3-dependent NF-κB signaling in response to UV and PMA (Massoumi et al., 2006). Thus, it is possible that CYLD functions in diverse pathways and loss of CYLD activity contributes to tumorigenesis via multiple mechanisms.

Lys63-linked ubiquitin chains, synthesized in response to cytokine-mediated activation of TNF receptor-associated factor (TRAF) 2 and TRAF6 E3 ubiquitin ligases, provide a common molecular scaffold for the coassembly of the transforming growth factor-β activated kinase-1 (TAK1) and inhibitor of NF-κB kinase (IKK) complexes (reviewed in Adhikari et al., 2007; Kovalenko and Wallach, 2006). Specific recognition of this ubiquitin polymer by the TAB2/3 subunit of TAK1 (Kanayama et al., 2004) and the NEMO/IKKγ subunit of IKK (Ea et al., 2006; Wu et al., 2006) promotes their coassociation, facilitating TAK1-mediated phosphorylation and activation of IKKβ and subsequent activation of the classical NF-κB pathway (reviewed in Kovalenko and Wallach, 2006). CYLD disassembles polyubiquitin chains attached to TRAF2, TRAF6, and NEMO (Brummelkamp et al., 2003; Kovalenko et al., 2003; Trompouki et al., 2003); however, both catalytic site and cancer-associated CYLD mutations are defective in their ability to antagonize NF-κB signaling and associated TRAF2/6 and NEMO deubiquitination. The direct interaction of CYLD with both TRAF2 and NEMO is facilitated by N-terminal

protein-protein interaction domains and contributes to its activity toward these substrates (Kovalenko et al., 2003; Saito et al., 2004; Trompouki et al., 2003).

Lys63-linked ubiquitination also plays a major role in endocytic pathways, which, together with monoubiquitination events, trigger the internalization and degradation or recycling, of cell-surface transmembrane proteins and growth factor receptors. In the internalization of the nerve growth factor receptor TrkA, siRNA-mediated suppression of CYLD causes sustained TrkA ubiquitination with Lys63 chains (Geetha et al., 2005). Furthermore, CYLD was found associated with the epidermal growth factor (EGF) receptor in response to EGF stimulation (Blagoev et al., 2004). Other substrates of CYLD include the protein kinase Lck (Reiley et al., 2006) and TRP cation channels (Stokes et al., 2006). With the exception of Lck (Reiley et al., 2006), CYLD-deubiquitinating activity is selective for Lys63-linked ubiquitin chains. Increasingly diverse roles for CYLD have recently been discovered. An RNA interference screen identified CYLD as a regulator of mitotic entry and an effector of DNA damage response pathways (Stegmeier et al., 2007). A direct interaction with the Plk1 protein kinase, together with common phenotypes caused by overexpression and loss of function of CYLD and Plk1, implicated Plk1 as a CYLD target. Strikingly, proteomic analysis identified more than 70 potential CYLD-interacting proteins and/or substrates (Stegmeier et al., 2007), the functional consequences of which are yet to be defined.

To understand the molecular basis of CYLD selectivity for Lys63-linked ubiquitin chains and to provide insights into cancer-associated CYLD mutations, we determined the crystal structure of the CYLD USP domain. We show that the CYLD Lys63-ubiquitin selectivity is endowed within the USP core, and mutational analysis identifies regions responsible for this specificity. In contrast to other DUBS, CYLD is able to hydrolyze Lys63-linked ubiquitin chains internally, an activity that might contribute to efficiently antagonizing signaling cascades. Surprisingly, the structure revealed a small Zn-binding module inserted within the catalytic domain, bearing structural similarities to B box domains and RING fingers of E3 ligases. We performed biochemical and bioinformatics analyses of this previously unknown type of B box domain, demonstrating a role in CYLD subcellular localization.

RESULTS AND DISCUSSION

Structure Determination

The *CYLD* gene encodes a protein of 956 amino acids with three N-terminal CAP-Gly domains and a C-terminal catalytic USP domain (Bignell et al., 2000). Biochemical and genetic analyses had previously indicated that a pathogenic truncated CYLD protein (Bignell et al., 2000), lacking the extreme C-terminal 20 amino acids (1–936), is catalytically inactive (Trompouki et al., 2003). Multiple sequence alignments, secondary structure prediction, and fold recognition programs were used to identify a putative N-terminal boundary for the USP domain. The resultant protein comprising the CYLD USP domain (residues 583–956) was produced using the baculovirus/insect cell system and purified to homogeneity for crystallization (see the Experimental Procedures).

Table 1. Data Collection and Refinement Statistics

	CYLD AuCN	CYLD Native
Data Collection Statistics		
Beamline	ID29	ID29
Wavelength (Å)	1.0396	1.040
Space group	$P2_12_12_1$	$P2_12_12_1$
Unit cell (Å)	a = 60.86	a = 60.49
	b = 89.06	b = 89.08
	c = 174.07	c = 171.81
Resolution (Å)	30–2.80 (2.95–2.80)	30–2.80 (2.95–2.80)
Observed reflections	94,731 (12,015)	80,656 (11,971)
Unique reflections	23,870 (3346)	23,405 (3374)
Redundancy	4.0 (3.6)	3.4 (3.5)
Completeness (%)	99.2 (97.9)	99.3 (99.8)
R_{merge}	0.072 (0.381)	0.100 (0.359)
$\langle I/\sigma I \rangle$	14.9 (2.9)	11.9 (2.3)
Phasing Statistics		
Resolution (Å)	30–3.00 (3.16–3.00)	
Anomalous completeness	95.6 (89.6)	
Anomalous multiplicity	2.1 (1.9)	
<FOM>	0.305	
Phasing power	0.914	
$\langle FOM \rangle_{DM}$ extended to 2.8 Å	0.560	
Refinement Statistics		
Reflections in test set		1412
R_{cryst}		0.235
R_{free}		0.281
Number of residues		675
Number of zinc ions		4
Number of waters		15
Wilson B ($Å^2$)		76.1
<B> protein ($Å^2$)		62.0
<B> waters ($Å^2$)		44.9
<B> ions ($Å^2$)		55.8
Rmsd from ideal geometry		
Bond length (Å)		0.008
Bond angles (°)		1.093
Ramachandran statistic (preferred/allowed/outliers)		549 (84%)/ 85(13%)/19 (3%)

Values between brackets are for the highest-resolution shell. All measured data were included in structure refinement.

The structure of the CYLD USP domain was determined at 2.8 Å resolution by X-ray crystallography, with phase information provided by a gold derivative (Table 1). The asymmetric unit of the CYLD crystal is formed from two molecules of the CYLD USP domain. Both domains are similarly well resolved and superimpose with an RMSD of 0.9 Å for equivalent Cα atoms. Some flexible surface loops are disordered in one or both molecules. Monomer

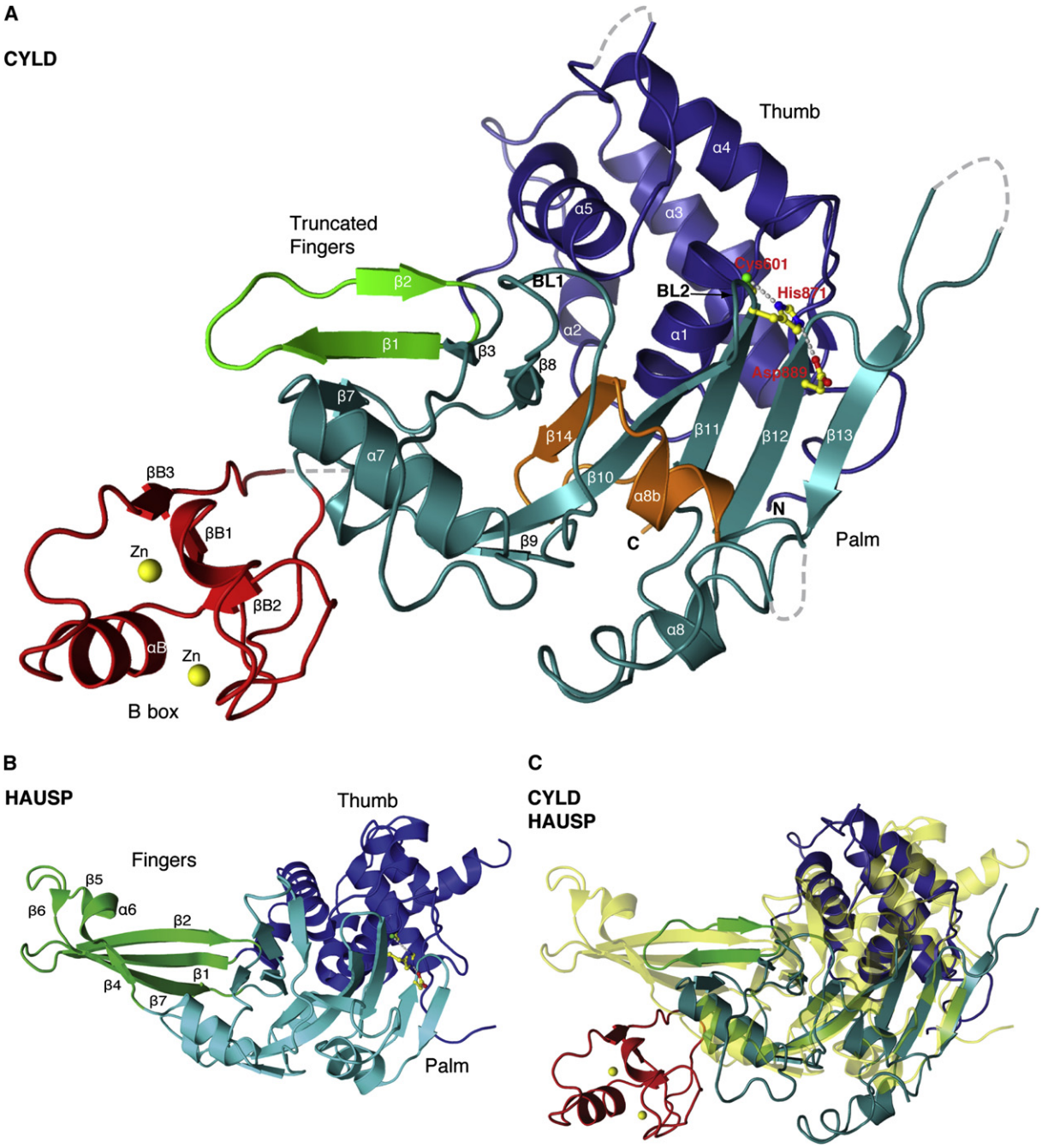

Figure 1. Structure of the CYLD USP Domain

(A) The CYLD USP domain is shown in cartoon representation, and subdomains are indicated in blue (Thumb), green (truncated Fingers), cyan (Palm), and red (B box). The C-terminal 20 amino acids, truncated in some cylindromatosis patients, are colored orange. Gray dotted lines indicate disordered loops. The two Zn atoms are shown as yellow spheres, and the Cys-His-Asp catalytic triad residues are shown.

(B) Structure of HAUSP using the same color scheme. Secondary structure elements in the Fingers domain that are not present in CYLD are labeled.

(C) Superposition of CYLD as in (A), with a yellow semitransparent model of active HAUSP. The molecules were superposed in coot (RMSD of 2.7 Å over 223 residues).

A is the slightly better ordered of the two and will provide the basis for our description (Figure 1A). Structures of six USP catalytic domains have previously been determined: HAUSP/USP7 (Hu et al., 2002), USP14 (Hu et al., 2005) and its yeast homolog Ubp6 (Protein Data Bank [PDB] 1vjv), bovine (Renatus et al., 2006) and human USP2 (PDB 1ibi), and USP8 (Avvakumov et al., 2006). Importantly, the DUB activity of all crystallized USP domains is associated with cleavage of Lys48-linked

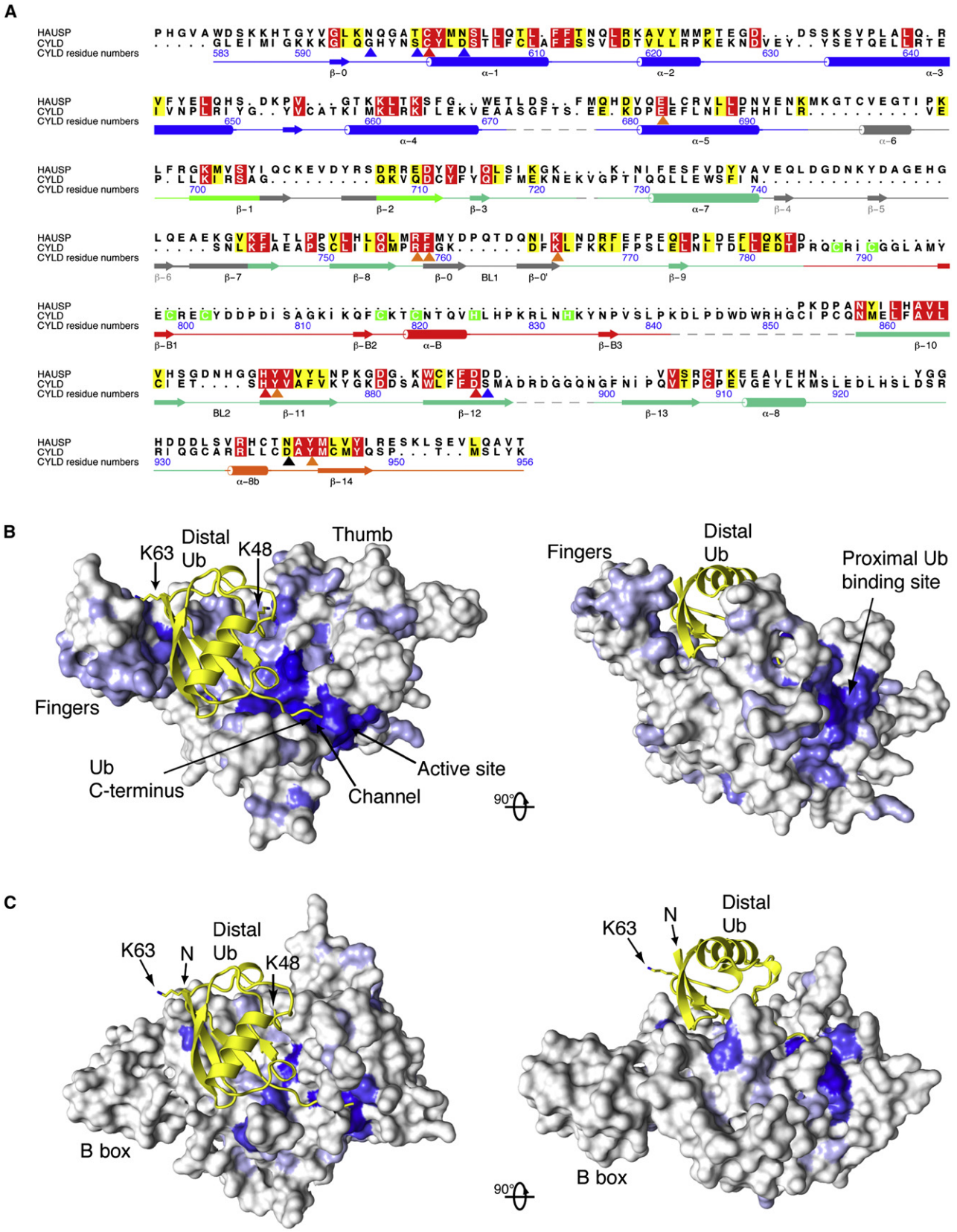
A
HAUSP
CYLD
CYLD residue numbers
B
K63
Distal Ub
K48
Thumb
Fingers
Ub C-terminus
Active site
Channel
90°
Fingers
Distal Ub
Proximal Ub binding site
C
K63
N
Distal Ub
K48
B box
90°
K63
N
Distal Ub
B box

ubiquitin chains; USP14 is unable to cleave Lys63-linked chains (Hu et al., 2005), and no such activity has been attributed to HAUSP, USP2, or USP8. The structural characterization of these USP domains has revealed a common architecture, with conserved catalytic residues forming a catalytic triad, reminiscent of other cysteinyl proteases (Amerik and Hochstrasser, 2004; Nijman et al., 2005). The structure of HAUSP (Hu et al., 2002) defined this common core and will serve as a comparison for CYLD in this study.

CYLD Domain Organization Differs from Other USPs

The USP domain of CYLD is organized into four subdomains strikingly different from previously determined USP structures. At the N terminus is a small α-helical subdomain of five α helices termed the Thumb. The second subdomain, the Palm, is dominated by a large nine-stranded β sheet and three α helices. These two domains are similar to their counterparts in other USPs (Figure 1) and incorporate the catalytic triad of Cys601, His871, and Asp889 (Figure 1A). The Cys residue, located at the N terminus of α1, functions as a nucleophile to undergo attack onto the isopeptide bond linking the C terminus of ubiquitin to the conjugated lysine residue, whereas the His and Asp residues, located on adjacent β strands of the Palm subdomain, activate the nucleophilic Cys. An oxyanion hole is created by the main-chain amides of residues surrounding the Cys and Asp residues (Figure 2A). A prominent channel is generated at the interface of the Thumb and Palm to engage the extended C-terminal residues of the distal ubiquitin moiety. Both the catalytic site and inter-Thumb-Palm cleft are highly conserved throughout the USP family (Figures 2B and 2C). The third "Fingers" subdomain is an extension of the Palm subdomain and in CYLD is greatly reduced in size compared with other USPs; the three β strands of HAUSP that extend the Palm subdomain are shortened (β1, β2, and β7) (Figure 2A), and CYLD lacks the three short strands (β4, β5, and β6) at the tip of the HAUSP Fingers (Figure 1). Another feature of CYLD is an additional subdomain characterized as a B box (see below), inserted between adjacent antiparallel β strands of the Palm.

Additional structural features that distinguish CYLD from other USPs include insertions and deletions of loops connecting elements of secondary structure (Figure 2A). Specifically, an insertion in the loop connecting the β12 and β13 strands significantly alters the enzyme's structure in the vicinity of the catalytic site (Figures 3D and 3E). The catalytic site of CYLD is predominantly preconfigured for catalysis, except that in molecule B, the side chain of the catalytic His871 is rotated out of hydrogen bond contact to the catalytic Cys601 and Asp889 residues. This suggests a small degree of conformational alteration at the active site on engaging substrate but contrasts markedly with the extensive conformational changes associated with HAUSP and some ubiquitin C-terminal hydrolases (Amerik and Hochstrasser, 2004; Hu et al., 2002). In CYLD, both the ubiquitin-binding loops, BL1 (β8/β9) and BL2, (β10/β11) that engage ubiquitin are considerably shorter than their counterparts in HAUSP and USP14 (Figures 2A and 3D, and see Figure S1 available online). Only BL1 (harboring Phe759 equivalent to the ubiquitin-interacting residue Phe409 of HAUSP) (Figure 2A) would be required to undergo a conformational change to engage ubiquitin. The BL1 loop exhibits a high degree of disorder in molecule B, and is also partly disordered in molecule A. In HAUSP, a loop connecting the α8 helix to β14 becomes ordered in the ubiquitin aldehyde complex. The equivalent loop of CYLD is longer and also disordered, and the position of the α8 helix differs from HAUSP (Figure 1).

Cancer-Associated Mutations Disrupt the USP Fold

Our structure of the CYLD USP domain provides a rationale of the structural consequences of cylindroma-associated mutations. The majority of pathological mutants lie within the USP domain, causing premature truncation of the protein (Bignell et al., 2000). All truncation-causing mutations disrupt the USP domain structure, thereby abrogating CYLD catalytic activity. This includes the extreme C-terminal mutation (R936X) that truncates the 20 amino acids that form an integral central strand (β14) of the Palm subdomain β sheet, and the adjacent α8b helix (Figures 1A and 2A).

The CYLD USP Domain Is Selective for Lys63-Linked Ubiquitin Chains

CYLD antagonizes cytokine-mediated signaling by hydrolyzing Lys63-linked ubiquitin chains. To determine whether the USP domain alone confers this substrate selectivity, we tested the capacity of the purified protein to disassemble Lys48 and Lys63-linked di- and tetraubiquitin in vitro. Figures 3A and 3B show that the CYLD USP catalytic domain (CYLDc) selectively hydrolyses Lys63-linked di- and tetraubiquitin but exhibits very little activity toward Lys48-linked polyubiquitin chains.

The selective disassembly of Lys63-linked diubiquitin indicates that specificity determinants for the isopeptide linkage are conferred by structural elements of the USP domain in the vicinity of the catalytic site, opposite to the catalytic site channel. We examined the conservation of surface residues lining the

Figure 2. Analysis of Structural Conservation between the CYLD and HAUSP USP Domains

(A) Structure-based sequence alignment highlighting conserved residues. Secondary structure elements are colored according to Figure 1A and labeled according to HAUSP. Gray elements correspond to the Fingers domain in HAUSP, and the B box insertion (residues 786–853) in CYLD including the eight Zn coordinating residues is shown in red. Disordered regions in molecule A are indicated by dotted lines. Residues of the catalytic triad and oxyanion hole are indicated with red and blue arrows, respectively, whereas conserved residues that contact ubiquitin are indicated with an orange arrow. Sequence alignment figures were prepared with Alscript (Barton, 1993).

(B) Conservation between CYLD, HAUSP, USP14, USP2, and Ubp6 is mapped onto the HAUSP surface with color ramp from white (nonconserved) to blue (conserved), and the ubiquitin molecule (from HAUSP) is shown in yellow. On the ubiquitin molecule, Lys63 and Lys48 are shown. The most conserved region comprises the channel that binds the C terminus of the distal ubiquitin. For a full alignment, refer to Figure S1.

(C) The conservation as in (B) is mapped onto the CYLD surface. The ubiquitin molecule from HAUSP is depicted; superposition of HAUSP (1nbf) and CYLD was performed in COOT.

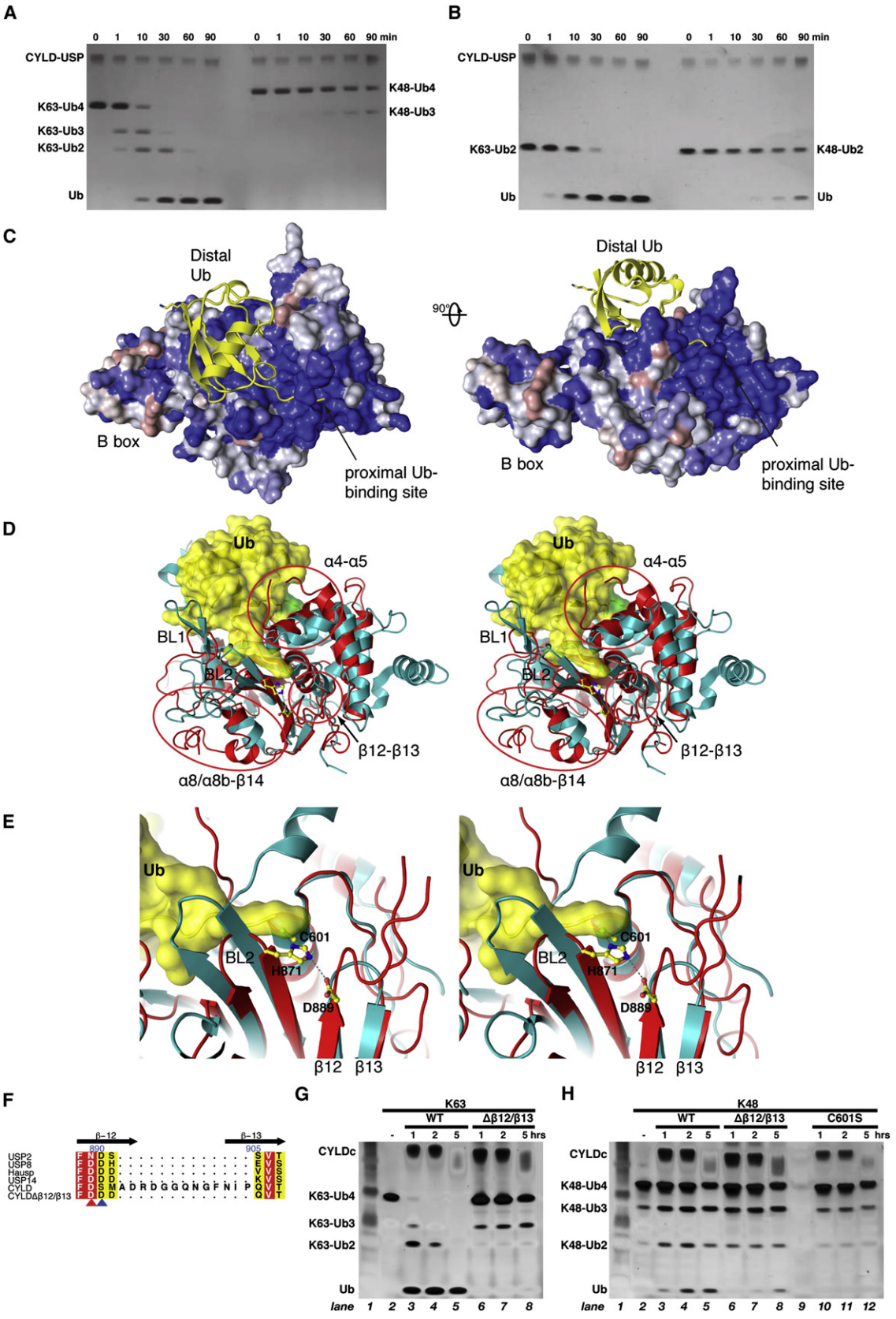
A
0 1 10 30 60 90 0 1 10 30 60 90 min
CYLD-USP
K63-Ub4
K63-Ub3
K63-Ub2
Ub
K48-Ub4
K48-Ub3
B
0 1 10 30 60 90 0 1 10 30 60 90 min
CYLD-USP
K63-Ub2
Ub
K48-Ub2
C
Distal Ub
B box
proximal Ub-binding site
90°
D
Ub
α4-α5
BL1
BL2
β12-β13
α8/α8b-β14
E
Ub
C601
BL2
H871
D889
β12
β13
F
β-12
β-13
890
905
USP2
USP8
Hausp
USP14
CYLD
CYLDΔβ12/β13
G
K63
WT
Δβ12/β13
- 1 2 5 1 2 5 hrs
CYLDc
K63-Ub4
K63-Ub3
K63-Ub2
Ub
lane 1 2 3 4 5 6 7 8
H
K48
WT
Δβ12/β13
C601S
- 1 2 5 1 2 5 1 2 5 hrs
CYLDc
K48-Ub4
K48-Ub3
K48-Ub2
Ub
lane 1 2 3 4 5 6 7 8 9 10 11 12

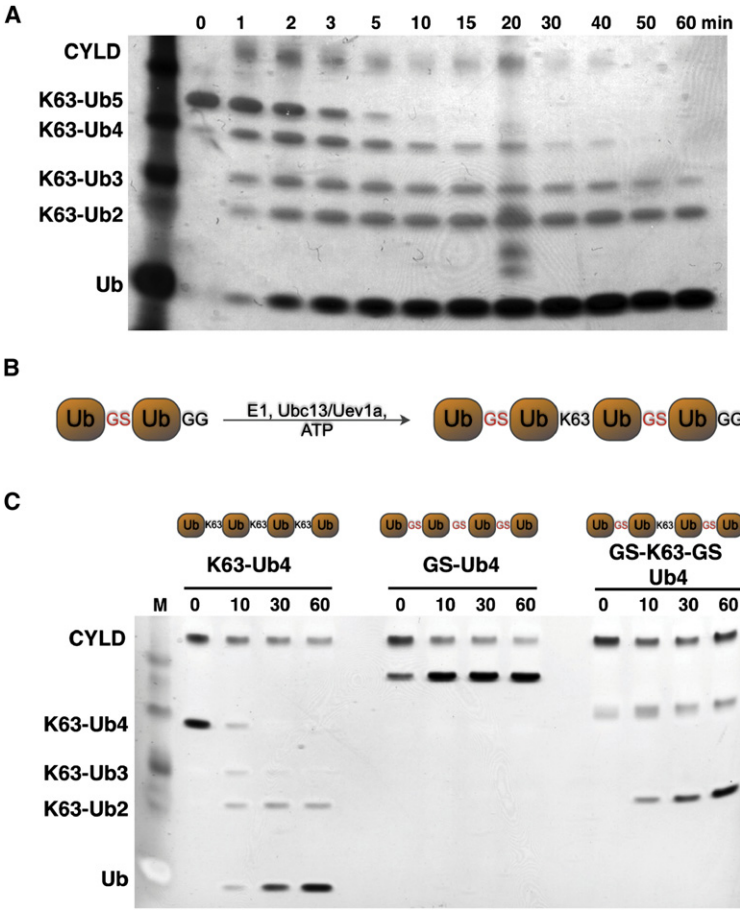

Figure 4. CYLD Has Endodeubiquitinase Activity

(A) Time course of DUB activity of CYLDc^{WT} for Lys63-linked pentaubiquitin. At any time point, equimolar amounts of all possible ubiquitin oligomers are produced, suggesting endodeubiquitinase activity.

(B) Preparation of a tetraubiquitin chain with noncleavable terminal linkages. A single Lys63-link is present between ubiquitin moieties 2 and 3 in the tetramer.

(C) CYLD activity against different forms of ubiquitin chains. CYLDc^{WT} fails to cleave a Gly-Ser (GS)-linked linear tetraubiquitin chain but dissembles a chain with a single internal Lys63-linkage.

proximal ubiquitin binding site (Figures 2B, 2C, and 3C). The proximal ubiquitin-binding site is well conserved between those USP domains with activity toward Lys48-linked polyubiquitin (Figure 2B). However, in CYLD, this site shares little similarity with other USP domains (Figure 2C), although it is markedly conserved among CYLD orthologs, consistent with a role in recognizing the proximal ubiquitin moiety of a Lys63-linked ubiquitin polymer (Figure 3C). Furthermore, variations in the conformations and size of the β12/β13, α4/α5, and α8/α8b-β14 (Figures 3D and 3E) loops of CYLD relative to other USPs could contribute to these specificity differences. We focused on the β12/β13 loop of CYLD, which is markedly extended compared to HAUSP and other USP domains (Figures 3E and 3F) but highly conserved in CYLD. To investigate the role of the β12/β13 loop in determining CYLD specificity, we truncated it to a size equivalent to the HAUSP β12/β13 loop (Figure 3F) and compared the specificity of the mutant and wild-type CYLDc (Figures 3G and 3H). Significantly, truncation of the β12/β13 loop almost completely abolished CYLD activity toward Lys63-linked chains (Figure 3G, compare lanes 3 and 6) but hardly affected the residual activity against Lys48-linked ubiquitin chains (Figure 3H, compare lanes 3 and 6), effectively rendering CYLD nonspecific. These data indicate that the extended β12/β13 loop of CYLD is a crucial structural determinant contributing to its specificity toward Lys63-linked ubiquitin chains.

CYLD Confers Endodeubiquitinase Activity for Lys63-Linked Ubiquitin Chains

Interestingly, analysis of the time-dependent hydrolysis of Lys63-linked pentaubiquitin (Figure 4A) indicated that all hydrolysis products are generated at similar rates, suggesting that CYLD is capable of cleaving all four isopeptide linkages equivalently. In contrast to CYLD, USP14 catalyzes the processive cleavage of the distal ubiquitin moiety of a Lys48-linked triubiquitin polymer and lacks significant activity toward Lys63-linked ubiquitin polymers (Hu et al., 2005). To further explore the

Figure 3. Substrate Specificity of CYLD

(A) CYLD specificity was tested in vitro against Lys63- and Lys48-linked tetraubiquitin chains (see the Experimental Procedures) in a time course experiment. CYLDc cleaves Lys63-linked ubiquitin chains at any internal linkage, while only triubiquitin is detectable in the case of Lys48 linked chains. At later time points (overnight), CYLDc disassembles all K48-tetraubiquitin to the monomer (data not shown).

(B) CYLDc is also specific for Lys63-linked diubiquitin over Lys48-linked diubiquitin, indicating that the specificity-determining environment is located in the active site region.

(C) Surface conservation within the CYLD USP domain from different species (found with accession numbers in Figure S2A), shown as in Figure 2 with a color ramp from red (nonconserved) to blue (conserved). The putative proximal ubiquitin binding site is highly conserved.

(D) Stereoview of CYLD (red) and HAUSP (green), with ubiquitin shown under a yellow surface. Differences between HAUSP and CYLD that might account for the observed specificity are circled, and the BL1 and BL2 loops are indicated.

(E) Closer view of the β12/β13 loop region in CYLD and HAUSP shown as in (D).

(F) Mutation of the β12/β13 loop in CYLD to the HAUSP equivalent.

(G and H) Specificity of CYLDc^{wt}, CYLDc$^{\Delta\beta12/\beta13}$, and CYLDc^{C601S} against Lys63 (G) and Lys48 (H) polyubiquitin.

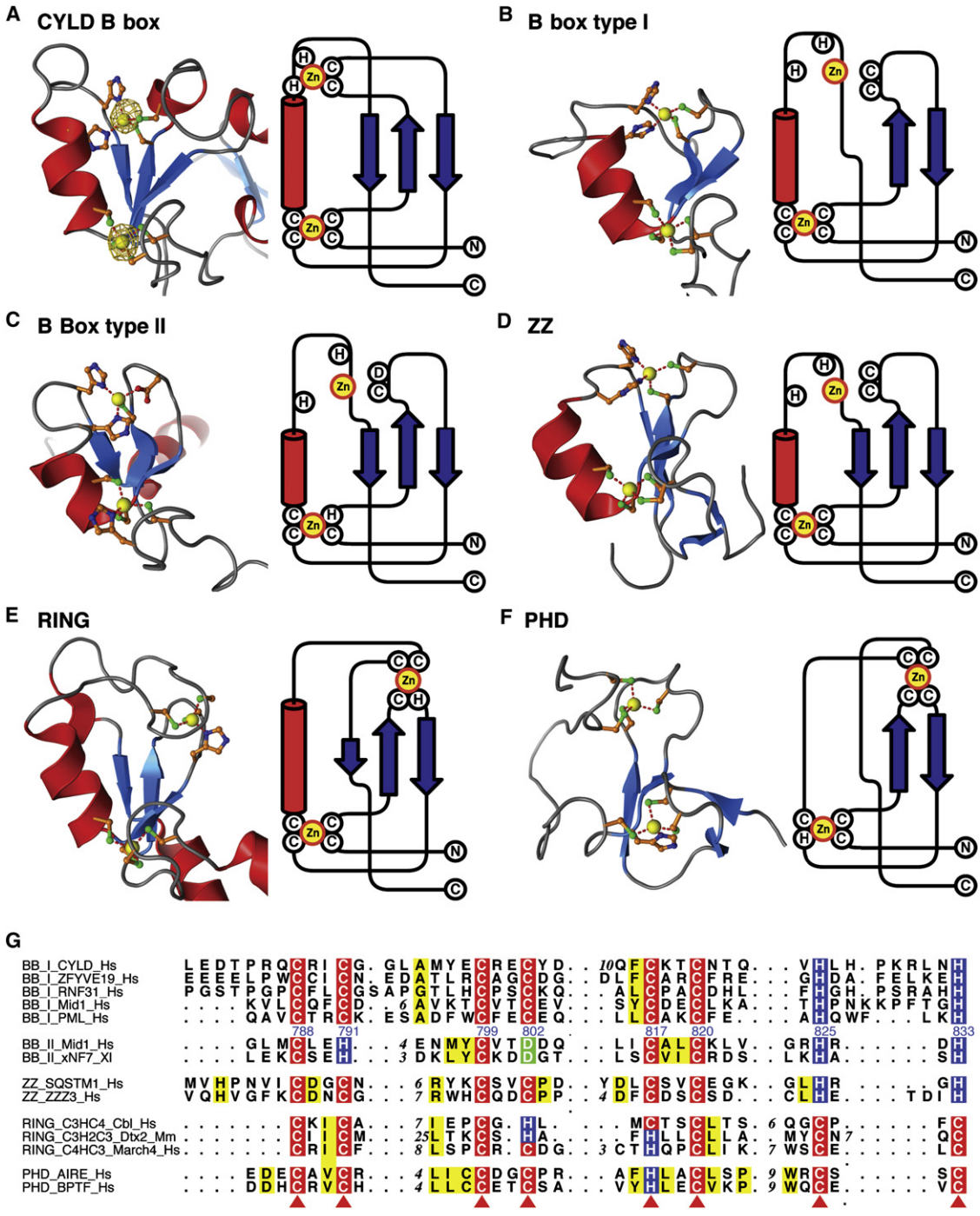

Figure 5. Analysis of the CYLD Zn-Binding Domain

Structural comparison of the CYLD Zn-binding domain with the most closely related structure revealed by DALI (Holm and Sander, 1993), and proteins with similar topology.

(A) CYLD Zn-binding domain. An anomalous difference map from data collected at the peak wavelength for Zn is drawn at 5σ indicating the Zn atoms.

(B) B box type I domain, PDB 2ffw (Massiah et al., 2006).

(C) B box type II domain, PDB 2d8v.

(D) ZZ domain, PDB 1tot (Legge et al., 2004).

(E) RING domain, PDB 2ckl (Buchwald et al., 2006).

(F) PHD domain, PDB 2g6q (Pena et al., 2006).

(G) Sequence alignment of the analyzed domains reveals that, despite similar folds, the order of Cys and His residues, the spacing between them, and additional conserved residues differentiate the families. Topology diagrams were generated with Topdraw (Bond, 2003).

endodeubiquitinase activity of CYLD, we generated a novel type of ubiquitin chain. We assembled Lys63-linked tetraubiquitin chains from noncleavable, linear ubiquitin dimers to generate tetraubiquitin oligomers with nonhydrolyzable terminal linkages (Figure 4B, Supplemental Experimental Procedures). Figure 4C shows that CYLD cleaved such chains producing nonhydrolyzable ubiquitin dimers, consistent with endocleavage activity. With the scissile Lys63 linkage of the tetraubiquitin polymer positioned at the catalytic site to enable cleavage into nonhydrolyzable ubiquitin dimers, we can rationalize the position of the most distal ubiquitin moiety (Figure 4B). Since the N terminus and Lys63 side chain of ubiquitin are in close proximity, the most distal ubiquitin moiety, attached to the N terminus of the adjacent ubiquitin moiety bound to the distal ubiquitin site of CYLD (Figure 2C), would occupy a position close to that expected for a distal Lys63-linked ubiquitin moiety. Potentially, endodeubiquitinase activity could be an important factor for CYLD's cellular functions by allowing efficient suppression of signaling cascades via releasing long chains from substrates.

In the structures of HAUSP, USP2, and USP14, in complex with ubiquitin and ubiquitin aldehyde, a prominent pocket within the USP domain accommodates the distal ubiquitin moiety (Hu et al., 2002, 2005; Renatus et al., 2006) (Figure 2B). With the channel at the Thumb and Palm interface engaging the extended C terminus of ubiquitin, the globular domain of ubiquitin is embraced by the pocket between α5 of the Thumb and the Fingers β sheet (Figure 2B). Significantly, the side chains of ubiquitin residues Lys48 and Lys63 are occluded by the Thumb and Fingers subdomains, respectively, suggesting that only the distal ubiquitin moiety of a polyubiquitin chain could be accommodated at this site and explaining the processive cleavage of the distal ubiquitin moiety by USP14 (Hu et al., 2005). In contrast, endoactivity is facilitated by the catalytic architecture of CYLD, in which the shortened Fingers subdomain exposes Lys63 on a bound distal ubiquitin, allowing chain elongation toward the distal end (Figures 2C and 3C). However, modeling indicates that, similar to HAUSP and USP14, the Lys48 side chain of the distal ubiquitin would be occluded and that a Lys48-linked chain could not be extended from a ubiquitin molecule bound to the distal ubiquitin binding site of CYLD (Figure 2C).

CYLD Contains a Zn-Binding Domain with Crossbrace Topology

An unexpected result of our structural analysis was the discovery of a structurally distinct subdomain of 60 amino acids (residues 782–842) (Figures 1 and 2A) inserted between the β9 and β10 strands of the Palm subdomain. The subdomain includes three Cys-x-x-Cys motifs, which, with a fourth pair of residues provided by two histidines, constitute two tetrahedrally coordinated metal binding sites (Figures 2A and 5G). The metal coordinating motifs are arranged in a crossbrace, in which the first and third binding motifs combine with the second and fourth motifs to generate the metal sites 1 and 2, respectively. In order to identify the endogenous metal ligand, we performed proton-induced X-ray emission (PIXE) experiments (Garman and Grime, 2005) with CYLDc, and the isolated metal-binding domain of CYLD (residues 778–842) expressed as a GST-fusion protein in *E. coli*, and purified without chelating agents. This quantitative analysis identified Zn unambiguously as a ligand of CYLD with a stoichiometry of two zinc atoms per protein molecule (data not shown). Subsequent purification of CYLD with the insect cell lysis buffer supplemented with 20 μM zinc sulfate enhanced the yield of soluble protein. Additionally, we performed X-ray fluorescence studies on native CYLD crystals, which revealed a strong fluorescent signal at the X-ray absorbance wavelength for Zn. An anomalous difference electron density map, calculated using a data set collected at the Zn absorbance edge, indicated strong electron density (11.5σ and 9.5σ peaks) corresponding to the positions of the first and second Zn binding sites, respectively (Figure 5A). We were therefore able to identify zinc as a physiological ligand of CYLD.

The Zn-Binding Domain of CYLD Resembles RING and B Box Proteins

Classification Based on Structure

We used DALI (Holm and Sander, 1993) to evaluate the protein data bank for the most similar structures to the Zn-binding module of CYLD (Figure 5A). This approach quantified fold similarities to the crossbrace Zn-binding domains of the two types of B box domains (Figures 5B and 5C), ZZ (Figure 5D), and RING domain (Figure 5E) (including the structurally similar U box proteins, which lack Zn-coordinating residues), although no similarity to PHD domains was revealed (Figure 5F). The most striking similarities with B box, ZZ, and RING/U box domains correspond to the first Zn-coordination site (located within 1 Å in the superposition). In contrast, the position of the second Zn ion is more variable (Figures 5A–5F). Analysis of loop arrangements and interzinc distances reveals that the CYLD Zn-binding domain is most similar in structure to B box type I domains, being less similar to B box type II and ZZ domains and least similar to RING domains, consistent with the highest correlation scores with B boxes in the DALI analysis.

Classification Based on Sequence

Despite the presence of a Zn-binding domain within CYLD, including three Cys-x-x-Cys motifs, sequence alignment and fold recognition programs failed to identify the B box subdomain. Sequence profiles for Zn-binding domains are commonly based on the type and spacing of Zn-coordinating residues and the presence of conserved amino acids. Our structural analysis reveals that CYLD comprises a C6H2 (six Cys, two His residues) architecture, with a seven amino acid spacing within the fourth motif. Because this pattern could not be recognized by currently available profiles, we used the generalized profile technique as a more sensitive protein sequence comparison method (Bucher et al., 1996). In accordance with the results from the structural analysis, sequence profiling revealed similarity of the CYLD Zn-binding domain to B box type I domains and, to a much lesser extent, to B box type II domains. No identifiable sequence similarity to RING, PHD, or ZZ domains apart from matching similar Zn-coordinating residues was observed (Figure 5G).

We used the derived CYLD B box profile to identify other CYLD-like B boxes by sequence similarities. Two families of proteins, RNF31/ZIBRA and ZFYVE19, with previously unannotated Zn-binding regions, can confidently be classified as B box-containing proteins (Figure 5G, see Supplemental Data and Figure S2).

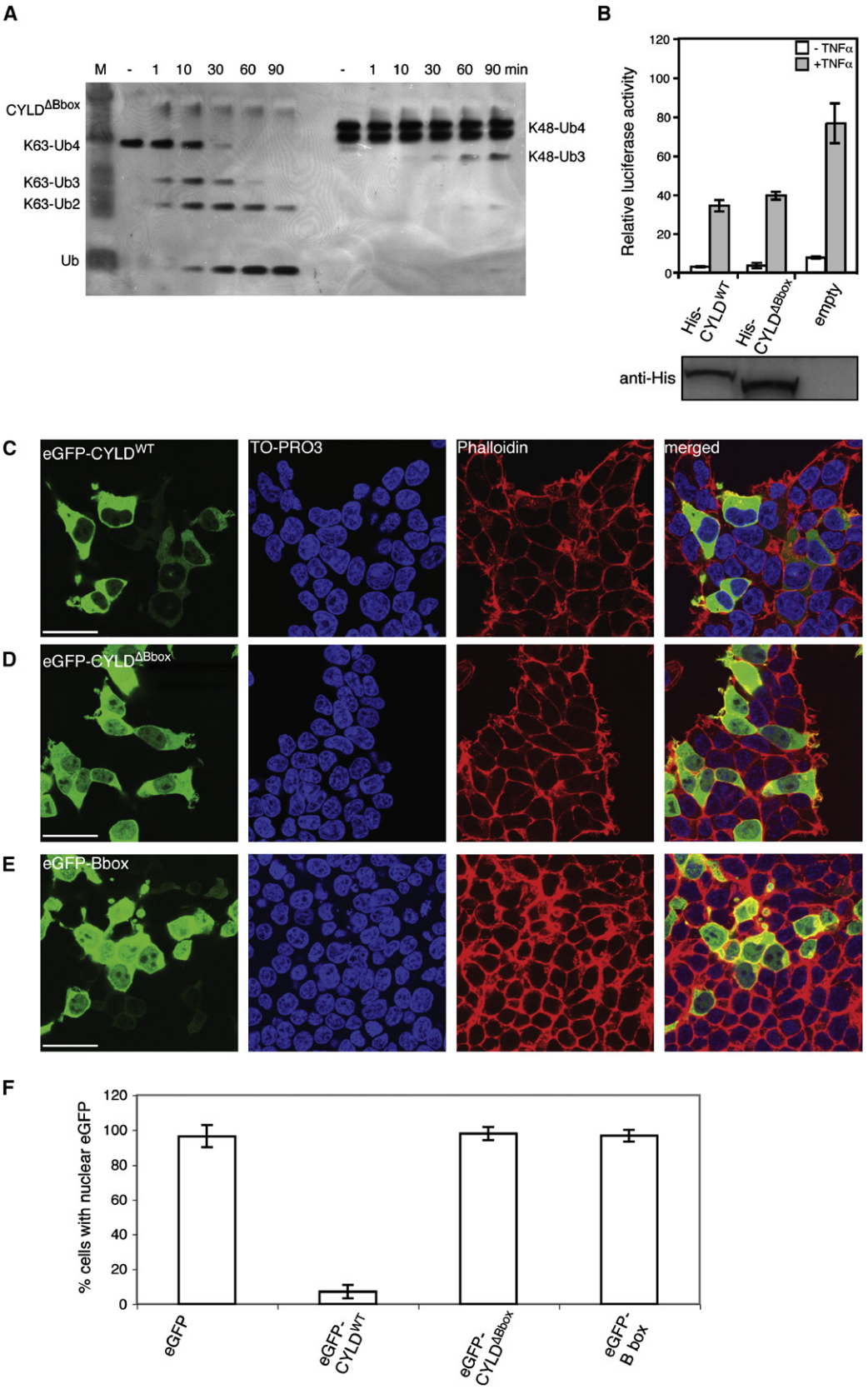
A
M - 1 10 30 60 90 - 1 10 30 60 90 min
CYLD^ΔBbox
K63-Ub4
K63-Ub3
K63-Ub2
Ub
K48-Ub4
K48-Ub3
B
Relative luciferase activity
- TNFα
+TNFα
His-CYLD^WT
His-CYLD^ΔBbox
empty
anti-His
C
eGFP-CYLD^WT
TO-PRO3
Phalloidin
merged
D
eGFP-CYLD^ΔBbox
E
eGFP-Bbox
F
% cells with nuclear eGFP
eGFP
eGFP-CYLD^WT
eGFP-CYLD^ΔBbox
eGFP-B box

CYLD Contains a B Box Domain—Functional Implications

Previously defined B box domains occur exclusively in tripartite motif (TRIM) family proteins. This highly conserved motif consists of a RING E3 ubiquitin ligase domain, followed by one or two B box domains, and a coil-coil region (reviewed in Meroni and Diez-Roux, 2005). Its presence at the N terminus of more than 100 human proteins, the spacing between domains, and late evolutionary origin suggest a highly specialized organization module (Meroni and Diez-Roux, 2005). Interestingly, all previously described B box type I domains occur in the TRIM motif in conjunction with B box type II domains. To our knowledge, the CYLD B box is therefore the first description of an isolated type I B box not in the context of a TRIM motif.

Little is known concerning the functions of B box domains within TRIM proteins. Direct and indirect roles in ubiquitination via the RING domain have been suggested (Massiah et al., 2006). Alternatively, the B box may function as a nonubiquitin-related protein-protein interaction domain. Consistent with this notion, the tandem B box modules of Mid1 mediate interactions with the C terminus of α4, a PP2A-regulatory subunit (Liu et al., 2001). Moreover, ZZ and RING domains also mediate protein-protein interactions (Ishikawa-Sakurai et al., 2004).

Function of the B Box in CYLD

To study the function of the CYLD B box, we replaced residues 776–855 with a Leu-Glu-Gly-Gly sequence (CYLD$^{\Delta Bbox}$). Such a substitution was possible, as the CYLD B box domain is inserted between strands β9 and β10 of the central β sheet of the USP core, which are less than 5 Å apart. The CYLD$^{\Delta Bbox}$ USP domain (CYLDc$^{\Delta Bbox}$) expressed at similar levels compared to CYLDc^{WT} in insect cells. For in vivo experiments, the same mutation was introduced into full-length CYLD for expression in mammalian cells.

The CYLD B Box Is Not Required for DUB Activity and Specificity

We performed in vitro deubiquitination assays with CYLDc$^{\Delta Bbox}$ (Figure 6A). CYLDc$^{\Delta Bbox}$ retains the same degree of activity and selectivity as CYLDc^{WT} (compare Figures 3A and 6A), indicating that the B box domain is not responsible for CYLD-deubiquitinating activity or ubiquitin chain selectivity and is not required for the proper folding of the catalytic domain. This is consistent with the location of the B box domain remote from the CYLD catalytic site and indicates that the minimal USP core, lacking the Fingers and B box subdomains, confers specificity for Lys63-linked ubiquitin chains.

These experiments do not exclude the possibility that the B box contributes indirectly to substrate deubiquitination by binding to (K63-linked) ubiquitin chains. We therefore tested whether the isolated GST-tagged CYLD B box could interact with ubiquitin, K63-linked tetraubiquitin, or K48-linked tetraubiquitin in pulldown experiments performed according to Ea et al. (2006). While we identified ubiquitin interactions with an unrelated ubiquitin-binding domain, we failed to observe an interaction of the GST-CYLD B box with either ubiquitin or ubiquitin chains (data not shown). We therefore suspect that the CYLD B box is not a ubiquitin-binding domain.

The CYLD B Box Has No E3 Ligase Activity

The structural similarities of B box domains and RING fingers, and the putative involvement of B boxes in ubiquitination, suggested the intriguing possibility that the CYLD B box confers E3 ligase activity, and that hence CYLD would combine both DUB and E3 ligase activities, similar to another regulator of NF-κB signaling, A20 (Wertz et al., 2004). However, in in vitro ubiquitination assays using a panel of 16 E2 enzymes representative of all subfamilies, we could not detect E3 ligase activity of His-tagged CYLDc or the isolated GST-tagged CYLD B box (Figures S3A and S3B).

Although our assay failed to demonstrate B box-mediated ubiquitination activity in vitro, the possibility existed that this could be due to the absence of the physiological substrate and/or E2. We therefore tested whether CYLDc binds to E2 enzymes in a directed yeast-two-hybrid (Y2H) screen against a library of 39 human E2 enzymes (Figure S3C) (Dodd et al., 2004). Using CYLDc as either bait or prey, none of the 39 E2s tested was capable of interacting sufficiently strongly, if at all, with CYLDc to obtain a positive Y2H response. Taken together, these approaches suggest that the B box of CYLD is unlikely to function as an E3 ligase in vivo.

The CYLD B Box Is Dispensable for NF-κB Suppression

Further analysis of the role of the CYLD B box was performed in HEK293 cells with full-length proteins. Overexpression of CYLD^{WT} inhibits activation of NF-κB-mediated transcription in response to TNFα stimulation (Figure 6B) (Kovalenko et al., 2003). The catalytically active CYLD$^{\Delta Bbox}$ mutant had the same inhibitory effect as CYLD^{WT} in these assays (Figure 6B), indicating that the CYLD B box is dispensable for CYLD-mediated suppression of TNFα-stimulated NF-κB activation. We also examined translocation of the NF-κB p65 subunit to the nucleus upon TNFα stimulation (Figure S4). In cells overexpressing GFP-tagged CYLD^{WT} or GFP-tagged CYLD$^{\Delta Bbox}$, p65 does not translocate to the nucleus, being retained in the cytoplasm (Figure S4). CYLD also affects Bcl3-mediated p50/p52 NF-κB

Figure 6. Role of the B Box Domain of CYLD

(A) Deubiquitination activity of CYLDc$^{\Delta Bbox}$, performed as in Figure 3A. CYLDc$^{\Delta Bbox}$ shows the same activity and specificity as CYLDc^{WT} in these assays.

(B) NF-κB activation in the presence of CYLD^{WT} and CYLD$^{\Delta Bbox}$. HEK293T cells were transfected with the 3XκBL and the pGK-β-galactosidase reporter plasmids in the presence of vectors expressing His-tagged full-length constructs of CYLD^{WT} and CYLD$^{\Delta Bbox}$. Twenty-four hours after transfection, NF-κB-mediated transcription was stimulated by addition of TNFα to the cell culture media, and luciferase and β-galactosidase activities were determined 6 hr later. Results are the mean ± standard deviation relative luciferase activity from three independent experiments. The inline picture shows representative immunoblots from lysates probed with anti-His antibody.

(C–E) Localization studies with eGFP-tagged CYLD^{WT} (C), eGFP-CYLD$^{\Delta Bbox}$ (D), and eGFP-B box (E) in HEK293T cells. Forty-eight hours after transfection, cellular eGFP was visualized by confocal microscopy alongside visualization of cell nuclei (using TO-PRO-3) and the cytoskeleton (by use of a fluorescently labeled phalloidin peptide that labels actin). The B box enables cytoplasmic retention of CYLD. A white bar represents a distance of 20 μm.

(F) Quantification of the number of cells with nuclear eGFP is shown, where data represent three independent transfections and mean and ± standard deviation values are shown.

activity (Massoumi et al., 2006). We did not observe a difference in p52 localization in response to TPA and UV treatment in HEK293 cells overexpressing either GFP-CYLD^{WT} or GFP-CYLD$^{\Delta Bbox}$, indicating that the B box does not influence the alternative NF-κB pathway in HEK293 cells (data not shown).

The B Box Determines Cytoplasmic Localization of CYLD

Recent data have shown that CYLD is located in the cytosol and adopts a punctuate pattern in the perinuclear region upon TPA stimulation (Massoumi et al., 2006). We investigated whether the B box affected localization of CYLD by transfecting GFP-fusion constructs of CYLD^{WT} and CYLD$^{\Delta Bbox}$ into HEK293 cells visualized by confocal imaging microscopy. Surprisingly, we found that, whereas CYLD^{WT} was indeed excluded from the nucleus, the CYLD$^{\Delta Bbox}$ mutant showed significant nuclear localization in all transfected cells, independently of TNFα stimulation (Figures 6C, 6D, and 6F and Figure S4). Hence, the CYLD B box contributes to retaining CYLD in the cytoplasm. The GFP-tagged isolated B box of CYLD was present in the cytoplasm and in the nucleus (Figure 6E). Therefore, the B box is necessary but not sufficient to retain CYLD in the cytoplasm of cells. To our knowledge, a specific role for B box domains in localization of TRIM proteins has not been studied.

Unlike the distinct localization of CYLD to subcellular compartments as shown by Massoumi et al. (2006), we observed a cytosolic distribution of CYLD^{WT} in unstimulated and TNFα-, TPA-, or UV-stimulated cells (Figure 6C and data not shown). This is likely to be a cell-type-specific effect (HEK293 cells in our study compared with primary keratinocytes). One mechanism for how the CYLD B box could affect localization is by mediating interactions with cytosolic proteins. The role of other crossbrace Zn-binding domains as protein interaction modules is consistent with such a notion, and the recent finding of numerous CYLD-interacting partners indicates that CYLD engages with multiple protein-protein interfaces (Stegmeier et al., 2007).

Concluding Remarks

The structure of the catalytic domain of the DUB CYLD has provided insights into the molecular basis for its specificity. Lack of a Fingers subdomain allows CYLD to hydrolyze internal linkages in a Lys63-linked polyubiquitin chain, providing a kinetic advantage for cleavage of this chain type compared to USP domains that only cleave from the distal end. In addition, differences in the active site environment, specifically the extended β12/β13 loop, contribute toward Lys63-linked specificity, whereas other differences account for the lack of activity toward Lys48-linked chains. These structural features are likely to be unique to CYLD, as, phylogenetically, it represents an outlier in the USP domain family (Nijman et al., 2005).

The B box fold inserted within the CYLD catalytic core was not previously predicted and may represent a paradigm for other USPs. The large size of many USP domains (up to 800 amino acids) contrasts with the relatively small USP core (~350 amino acids) and suggests that extradomain insertions are a common feature of the family. Our experiments indicate the feasibility of removing such inserted domains yielding active and stable protein, which might prove beneficial for further structural analysis of USP family members.

The occurrence of the isolated B box in CYLD allows the functional characterization of this module outside of the TRIM context. All our data are consistent with a function in protein-protein interactions. Further experiments and protein complex determination will be required to elucidate the precise role of the newly discovered B box domain in CYLD.

EXPERIMENTAL PROCEDURES

Protein Production and Purification

Generation of recombinant baculovirus for human CYLD (residues 583–956) using the GIBCO/Life Sciences Bacmid system was performed using standard procedures and used to infect *Sf*9 cells at a MOI of 2 for 72 hr. Protein purification was performed at 4°C. Cells were harvested and lysed in lysis buffer (300 mM sodium chloride, 25 mM Tris [pH 8.0], 15 mM imidazole). The cleared lysate was subjected to affinity chromatography using TALON Sepharose (BD Biosciences). His_6-CYLD was eluted with elution buffer (300 mM sodium chloride, 25 mM Tris [pH 7.0], 300 mM imidazole), and the His_6-tag was cleaved overnight with 100 μg GST-PreScission protease in buffer A (200 mM sodium chloride, 25 mM Tris [pH 8.5], 5 mM DTT). GST-PreScission protease was removed using GSH-Sepharose, and CYLD was subjected to anion exchange (MonoQ) and gel filtration in buffer A.

Crystallization, Data Collection, Phasing, and Refinement

Screening for crystallization conditions was performed in a sitting-drop setup at 20°C with CYLD at 10 mg/ml. Small plate-cluster crystals were obtained overnight in 5% PEG 20000, 0.1 M MES (pH 6.5). Subsequent refinement of conditions gave large, but thin, single plate crystals from mother liquor containing 1.5%–2% PEG 20000, 0.1 M MES (pH 6.3). Prior to freezing in a nitrogen cryostream, the crystals were soaked in mother liquor containing 25% MPD.

Diffraction data on CYLD were collected at the ESRF (Grenoble, France), beamline ID-29. The crystals belong to the space group $P2_12_12_1$, with two molecules per asymmetric unit (Table 1). The presence of a reactive active-site cysteine residue was employed for phasing by heavy atoms, using derivatization with AuCN. For this, single crystals were soaked in a mother liquor containing 1 mM AuCN for 25 min prior to the freezing procedure. A SAD data set to 3.0 Å was collected, and, using SHELX/hkl2map (Pape and Schneider, 2004), 12 heavy atom sites were identified. These sites were subsequently refined with autoSHARP (Bricogne et al., 2003), and the SHARP solvent-flattening procedure resulted in high-quality maps. A native data set was collected to 2.8 Å resolution. The protein was built using COOT (Emsley and Cowtan, 2004) and refined using PHENIX, including simulated annealing and TLS B factor refinement (Adams et al., 2002). In molecule A, the surface loops 671–678, 723–723, 841–857, and 893–899 are disordered, while, in molecule B, residues 672–679, 719–727, 759–766, 894–901, 929–934, and 956 lacked electron density. Final statistics are listed in Table 1. A fluorescent scan on Zn edge indicated bound Zn atoms even in the native crystals, and a data set at the peak wavelength for Zn resulted in 9–11 σ peaks in the anomalous difference maps for all four Zn atoms in the asymmetric unit (Figure 5A).

In Vitro Deubiquitination Assays

In vitro deubiquitination assays were performed with 1.5 μg of CYLDc^{WT} or indicated CYLDc mutants, 2.5 μg Lys63- or Lys48-tetraubiquitin chains as substrate, in 30 μl DUB buffer (50 mM Tris [pH7.6], 5 mM DTT) at 37°C. Aliquots (5 μl) of the reaction were taken at the time points indicated, and the reaction was stopped by addition of 2× SDS-sample loading buffer. Samples were subjected to SDS PAGE analysis with subsequent silver staining using the Bio-Rad Silver Stain Plus Kit with the manufacturer's protocol.

Confocal Microscopy

HEK293T cells were transfected with vectors expressing eGFP-tagged versions of full-length CYLD with and without the B box (eGFP-CYLD^{WT}/eGFP-CYLD$^{\Delta Bbox}$). Forty-eight hours after transfection, cells were fixed on glass coverslips using 4% (w/v) paraformaldehyde. Fixed cells were washed in PBS and then permeabilized using 0.2% (v/v) Triton X-100/PBS. Cells were stained with a 1:10,000 dilution of Alexa-Fluor-635 phalloidin (Invitrogen) to detect cytoskeletal actin, and TO-PRO-3 iodide (Invitrogen) to enable visualization of nuclei. Cells were visualized using a Leica TCS-SP2 confocal microscope.

Additional Experimental Procedures can be found in the Supplemental Data online.

ACCESSION NUMBERS

Coordinates and structure factors have been deposited in the Protein Data Bank under accession number 2vhf.

SUPPLEMENTAL DATA

Supplemental Data include supplemental text, four figures, Supplemental Experimental Procedures, and Supplemental References and can be found with this article online at http://www.molecule.org/cgi/content/full/29/4/451/DC1/.

ACKNOWLEDGMENTS

We thank Elspeth Garman (Oxford) for the PIXE experiments; Chris Sanderson (Liverpool) for the Y2H analysis; Jane Endicott (Oxford), Philip Cohen, and Neil Perkins (Dundee) for constructs and reagents; and Richard Elliott (ICR) and Neil Perkins for helpful discussions. This work was funded by Cancer Research UK and Breakthrough Breast Cancer. D.K. is funded by a Beit Memorial Fellowship for Medical Research.

Received: July 11, 2007
Revised: October 24, 2007
Accepted: December 6, 2007
Published: February 28, 2008

REFERENCES

Adams, P.D., Grosse-Kunstleve, R.W., Hung, L.W., Ioerger, T.R., McCoy, A.J., Moriarty, N.W., Read, R.J., Sacchettini, J.C., Sauter, N.K., and Terwilliger, T.C. (2002). PHENIX: building new software for automated crystallographic structure determination. Acta Crystallogr. D Biol. Crystallogr. *58*, 1948–1954.

Adhikari, A., Xu, M., and Chen, Z.J. (2007). Ubiquitin-mediated activation of TAK1 and IKK. Oncogene *26*, 3214–3226.

Amerik, A.Y., and Hochstrasser, M. (2004). Mechanism and function of deubiquitinating enzymes. Biochim. Biophys. Acta *1695*, 189–207.

Avvakumov, G.V., Walker, J.R., Xue, S., Finerty, P.J., Jr., Mackenzie, F., Newman, E.M., and Dhe-Paganon, S. (2006). Amino-terminal dimerization, NRDP1-rhodanese interaction, and inhibited catalytic domain conformation of the ubiquitin-specific protease 8 (USP8). J. Biol. Chem. *281*, 38061–38070.

Barton, G.J. (1993). ALSCRIPT: a tool to format multiple sequence alignments. Protein Eng. *6*, 37–40.

Biggs, P.J., Wooster, R., Ford, D., Chapman, P., Mangion, J., Quirk, Y., Easton, D.F., Burn, J., and Stratton, M.R. (1995). Familial cylindromatosis (turban tumour syndrome) gene localised to chromosome 16q12-q13: evidence for its role as a tumour suppressor gene. Nat. Genet. *11*, 441–443.

Bignell, G.R., Warren, W., Seal, S., Takahashi, M., Rapley, E., Barfoot, R., Green, H., Brown, C., Biggs, P.J., Lakhani, S.R., et al. (2000). Identification of the familial cylindromatosis tumour-suppressor gene. Nat. Genet. *25*, 160–165.

Blagoev, B., Ong, S.E., Kratchmarova, I., and Mann, M. (2004). Temporal analysis of phosphotyrosine-dependent signaling networks by quantitative proteomics. Nat. Biotechnol. *22*, 1139–1145.

Bond, C.S. (2003). TopDraw: a sketchpad for protein structure topology cartoons. Bioinformatics *19*, 311–312.

Bricogne, G., Vonrhein, C., Flensburg, C., Schiltz, M., and Paciorek, W. (2003). Generation, representation and flow of phase information in structure determination: recent developments in and around SHARP 2.0. Acta Crystallogr. D Biol. Crystallogr. *59*, 2023–2030.

Brummelkamp, T.R., Nijman, S.M., Dirac, A.M., and Bernards, R. (2003). Loss of the cylindromatosis tumour suppressor inhibits apoptosis by activating NF-kappaB. Nature *424*, 797–801.

Bucher, P., Karplus, K., Moeri, N., and Hofmann, K. (1996). A flexible motif search technique based on generalized profiles. Comput. Chem. *20*, 3–23.

Buchwald, G., van der Stoop, P., Weichenrieder, O., Perrakis, A., van Lohuizen, M., and Sixma, T.K. (2006). Structure and E3-ligase activity of the Ring-Ring complex of polycomb proteins Bmi1 and Ring1b. EMBO J. *25*, 2465–2474.

Chen, Z.J. (2005). Ubiquitin signalling in the NF-kappaB pathway. Nat. Cell Biol. *7*, 758–765.

Deng, L., Wang, C., Spencer, E., Yang, L., Braun, A., You, J., Slaughter, C., Pickart, C., and Chen, Z.J. (2000). Activation of the IkappaB kinase complex by TRAF6 requires a dimeric ubiquitin-conjugating enzyme complex and a unique polyubiquitin chain. Cell *103*, 351–361.

Dodd, R.B., Allen, M.D., Brown, S.E., Sanderson, C.M., Duncan, L.M., Lehner, P.J., Bycroft, M., and Read, R.J. (2004). Solution structure of the Kaposi's sarcoma-associated herpesvirus K3 N-terminal domain reveals a novel E2-binding C4HC3-type RING domain. J. Biol. Chem. *279*, 53840–53847.

Ea, C.K., Deng, L., Xia, Z.P., Pineda, G., and Chen, Z.J. (2006). Activation of IKK by TNFalpha requires site-specific ubiquitination of RIP1 and polyubiquitin binding by NEMO. Mol. Cell *22*, 245–257.

Emsley, P., and Cowtan, K. (2004). Coot: model-building tools for molecular graphics. Acta Crystallogr. D Biol. Crystallogr. *60*, 2126–2132.

Garman, E.F., and Grime, G.W. (2005). Elemental analysis of proteins by microPIXE. Prog. Biophys. Mol. Biol. *89*, 173–205.

Geetha, T., Jiang, J., and Wooten, M.W. (2005). Lysine 63 polyubiquitination of the nerve growth factor receptor TrkA directs internalization and signaling. Mol. Cell *20*, 301–312.

Hellerbrand, C., Bumes, E., Bataille, F., Dietmaier, W., Massoumi, R., and Bosserhoff, A.K. (2007). Reduced expression of CYLD in human colon and hepatocellular carcinomas. Carcinogenesis *28*, 21–27.

Holm, L., and Sander, C. (1993). Protein structure comparison by alignment of distance matrices. J. Mol. Biol. *233*, 123–138.

Hu, M., Li, P., Li, M., Li, W., Yao, T., Wu, J.W., Gu, W., Cohen, R.E., and Shi, Y. (2002). Crystal structure of a UBP-family deubiquitinating enzyme in isolation and in complex with ubiquitin aldehyde. Cell *111*, 1041–1054.

Hu, M., Li, P., Song, L., Jeffrey, P.D., Chenova, T.A., Wilkinson, K.D., Cohen, R.E., and Shi, Y. (2005). Structure and mechanisms of the proteasome-associated deubiquitinating enzyme USP14. EMBO J. *24*, 3747–3756.

Ikeda, F., and Dikic, I. (2006). CYLD in ubiquitin signaling and tumor pathogenesis. Cell *125*, 643–645.

Ishikawa-Sakurai, M., Yoshida, M., Imamura, M., Davies, K.E., and Ozawa, E. (2004). ZZ domain is essentially required for the physiological binding of dystrophin and utrophin to beta-dystroglycan. Hum. Mol. Genet. *13*, 693–702.

Jin, W., Reiley, W.R., Lee, A.J., Wright, A., Wu, X., Zhang, M., and Sun, S.C. (2007). Deubiquitinating enzyme CYLD regulates the peripheral development and naive phenotype maintenance of B cells. J. Biol. Chem. *282*, 15884–15893.

Kanayama, A., Seth, R.B., Sun, L., Ea, C.K., Hong, M., Shaito, A., Chiu, Y.H., Deng, L., and Chen, Z.J. (2004). TAB2 and TAB3 activate the NF-kappaB pathway through binding to polyubiquitin chains. Mol. Cell *15*, 535–548.

Kovalenko, A., and Wallach, D. (2006). If the prophet does not come to the mountain: dynamics of signaling complexes in NF-kappaB activation. Mol. Cell *22*, 433–436.

Kovalenko, A., Chable-Bessia, C., Cantarella, G., Israel, A., Wallach, D., and Courtois, G. (2003). The tumour suppressor CYLD negatively regulates NF-kappaB signalling by deubiquitination. Nature *424*, 801–805.

Legge, G.B., Martinez-Yamout, M.A., Hambly, D.M., Trinh, T., Lee, B.M., Dyson, H.J., and Wright, P.E. (2004). ZZ domain of CBP: an unusual zinc finger fold in a protein interaction module. J. Mol. Biol. *343*, 1081–1093.

Liu, J., Prickett, T.D., Elliott, E., Meroni, G., and Brautigan, D.L. (2001). Phosphorylation and microtubule association of the Opitz syndrome protein mid-1 is regulated by protein phosphatase 2A via binding to the regulatory subunit alpha 4. Proc. Natl. Acad. Sci. USA *98*, 6650–6655.

Massiah, M.A., Simmons, B.N., Short, K.M., and Cox, T.C. (2006). Solution structure of the RBCC/TRIM B-box1 domain of human MID1: B-box with a RING. J. Mol. Biol. *358*, 532–545.

Massoumi, R., Chmielarska, K., Hennecke, K., Pfeifer, A., and Fassler, R. (2006). Cyld inhibits tumor cell proliferation by blocking Bcl-3-dependent NF-kappaB signaling. Cell *125*, 665–677.

Meroni, G., and Diez-Roux, G. (2005). TRIM/RBCC, a novel class of 'single protein RING finger' E3 ubiquitin ligases. Bioessays *27*, 1147–1157.

Nijman, S.M., Luna-Vargas, M.P., Velds, A., Brummelkamp, T.R., Dirac, A.M., Sixma, T.K., and Bernards, R. (2005). A genomic and functional inventory of deubiquitinating enzymes. Cell *123*, 773–786.

Pape, T., and Schneider, T.R. (2004). Hkl2map: a graphical user interface for macromolecular phasing with shelx programs. J. Appl. Cryst. *37*, 843–844.

Pena, P.V., Davrazou, F., Shi, X., Walter, K.L., Verkhusha, V.V., Gozani, O., Zhao, R., and Kutateladze, T.G. (2006). Molecular mechanism of histone H3K4me3 recognition by plant homeodomain of ING2. Nature *442*, 100–103.

Reiley, W.W., Zhang, M., Jin, W., Losiewicz, M., Donohue, K.B., Norbury, C.C., and Sun, S.C. (2006). Regulation of T cell development by the deubiquitinating enzyme CYLD. Nat. Immunol. *7*, 411–417.

Renatus, M., Parrado, S.G., D'Arcy, A., Eidhoff, U., Gerhartz, B., Hassiepen, U., Pierrat, B., Riedl, R., Vinzenz, D., Worpenberg, S., et al. (2006). Structural basis of ubiquitin recognition by the deubiquitinating protease USP2. Structure *14*, 1293–1302.

Saito, K., Kigawa, T., Koshiba, S., Sato, K., Matsuo, Y., Sakamoto, A., Takagi, T., Shirouzu, M., Yabuki, T., Nunokawa, E., et al. (2004). The CAP-Gly domain of CYLD associates with the proline-rich sequence in NEMO/IKKgamma. Structure *12*, 1719–1728.

Stegmeier, F., Sowa, M.E., Nalepa, G., Gygi, S.P., Harper, J.W., and Elledge, S.J. (2007). The tumor suppressor CYLD regulates entry into mitosis. Proc. Natl. Acad. Sci. USA *104*, 8869–8874.

Stokes, A., Wakano, C., Koblan-Huberson, M., Adra, C.N., Fleig, A., and Turner, H. (2006). TRPA1 is a substrate for de-ubiquitination by the tumor suppressor CYLD. Cell. Signal. *18*, 1584–1594.

Sun, L., and Chen, Z.J. (2004). The novel functions of ubiquitination in signaling. Curr. Opin. Cell Biol. *16*, 119–126.

Trompouki, E., Hatzivassiliou, E., Tsichritzis, T., Farmer, H., Ashworth, A., and Mosialos, G. (2003). CYLD is a deubiquitinating enzyme that negatively regulates NF-kappaB activation by TNFR family members. Nature *424*, 793–796.

van Balkom, I.D., and Hennekam, R.C. (1994). Dermal eccrine cylindromatosis. J. Med. Genet. *31*, 321–324.

Wertz, I., O'Rourke, K., Zhou, H., Eby, M., Aravind, L., Seshagiri, S., Wu, P., Wiesmann, C., Baker, R., Boone, D., et al. (2004). De-ubiquitination and ubiquitin ligase domains of A20 downregulate NF-kappaB signalling. Nature *430*, 694–699.

Wu, C.J., Conze, D.B., Li, T., Srinivasula, S.M., and Ashwell, J.D. (2006). Sensing of Lys 63-linked polyubiquitination by NEMO is a key event in NF-kappaB activation. Nat. Cell Biol. *8*, 398–406.

Zhang, J., Stirling, B., Temmerman, S.T., Ma, C.A., Fuss, I.J., Derry, J.M., and Jain, A. (2006). Impaired regulation of NF-kappaB and increased susceptibility to colitis-associated tumorigenesis in CYLD-deficient mice. J. Clin. Invest. *116*, 3042–3049.